Fe_3O_4 Nanoparticles and Carboxymethyl Cellulose: A Green Option for the Removal of Atmospheric Benzene, Toluene, Ethylbenzene, and *o*-Xylene (BTEX)

Nermin A. Eltouny and Parisa A. Ariya*†‡

Abstract

In this work, we investigate the interaction of gaseous benzene, toluene, ethylbenzene, and *o*-xylene (BTEX) with Fe_3O_4 nanoparticles and demonstrate the potential application of Fe_3O_4 nanoparticles as adsorbents for BTEX. On the basis of X-ray diffraction, transmission electron microscopy, gas chromatography–mass spectrometry, and gas chromatography–flame ionization detection results, using toluene as a model compound, we find that adsorption is of a heterogeneous nature. At relatively high concentrations of toluene (300–2790 ppmv), X-ray photoelectron spectroscopy results indicate an increase in the divalent cations relative to the trivalent cations of Fe_3O_4 nanoparticles, which is possibly triggered by nanoscale effects. Removal efficiency experiments show that Fe_3O_4 nanoparticles (4 g) reduce 100 ppmv of BETX in air by 83 ± 8%, 95 ± 5%, 97 ± 1%, and 98 ± 2%, respectively. Comparable removal efficiencies were observed for recycled Fe_3O_4 nanoparticles. Toluene was also removed from a flow by Fe_3O_4 nanoparticles bound together with carboxymethyl cellulose, without releasing undesired aerosols. Fe_3O_4 nanoparticles (bare and as a composite) show potential as practical and environmental friendly materials for the remediation of BTEX from air.

Introduction

Magnetite is a naturally occurring iron oxide that is relevant to biology,(1) environmental remediation(2) and heterogeneous catalysis(3) among others fields. Understanding the interactions between magnetite and various compounds is essential for many of those applications and in particular for environmental remediation and heterogeneous catalysis. Numerous studies have focused on the fundamental understanding under specific conditions such as the dissociative adsorption of CO, CO_2,(4) and H_2O(5) and the acid base interactions between monosubstituted benzene and FeO,(6) a related oxide. Other studies have focused on catalytic conditions such as those required for the dehydrogenation of ethylbenzene by magnetite.(3) A current interest in magnetite relates to investigating the nanoscale effect on properties such as adsorption capacity,(2) oxidation reduction potential(7) and magnetism.(8)

Monosubstituted benzenes such as toluene and ethylbenzene constitute, in addition to benzene and xylenes, the group of organic compounds known as BTEX, one class of volatile organic compounds (VOCs), which are an important category of air pollutants. Although they are mostly released from biogenic sources such as plants,(9) VOCs also have anthropogenic origins, most of which have been attributed to the transport and industrial sectors, and to biomass burning.(10) The release of VOCs has several impacts on the atmosphere. VOCs can undergo (photo) chemistry, resulting in the formation of aerosols, the alteration of the oxidation potential of the lower atmosphere, and in the presence of nitrogen oxides, in the formation of ozone, a principal component of photochemical smog that degrades regional air quality.(9) Both ozone and aerosols also influence the climate as they influence the Earth's radiative balance.(9) The detrimental impacts of VOCs extend to posing threats on human health(11) especially in environments bordering high-traffic streets.(12)

Investigating interactions of BTEX and magnetite nanoparticles (NPs) at ambient conditions (i.e., room temperature and pressure) could have potential applications for the remediation of polluted air by adsorption as well implications for atmospheric reactions on dusts.(13) Recent efforts to treat BTEX have been dedicated to developing adsorption materials to overcome challenges faced by conventional adsorbents like activated carbon and zeolites.(14) Materials such as carbon nanotubes and ordered mesoporous silicas have been suggested as they offer improved adsorption features; yet, the complexity and inherent formation of wastes during their synthesis are a subject of environmental concern for large scale production.(15-17) The synthesis and application of adsorbents should thereby be simple and

environmental friendly. In this context, magnetite has several attractive features. It can be simply synthesized without using organic solvents or producing hazardous wastes(18, 19) and its magnetic properties could be used at various stages of the process (transport, collection and recycling) by applying a magnetic field. For remediation purposes, magnetite is known for the removal of heavy metals from polluted waters.(20, 21) With respect to organic compounds, magnetite has been reported for the reduction of nitrobenzene in aqueous media(22) and the dehydrogenation of ethylbenzene.(3) However, its properties have not been explored for the adsorption of gaseous BTEX at room temperature and pressure.

Herein, we report our investigation of selected VOCs, at room temperature (296 ± 2 K) and atmospheric pressure (~740 ± 20 Torr), from the perspective of fundamental and applied science, onto heterogeneous mesoporous magnetite nanoparticles. To the best of our knowledge it is a first study of the kind. Our aim was to determine (1) the interaction of various VOCs, using toluene as a model BTEX, with nanoparticles, (2) the adsorption mechanism, and (3) the capacity and applicability of Fe_3O_4 NPs, bare and within a composite, using carboxymethyl cellulose as a binder (CMC–Fe_3O_4 NPs), to be applied in real conditions in removing BTEX gaseous pollutants.

EXPERIMENTAL SECTIONS

Characterizations of the Adsorbents

We used several complementary analytical techniques to characterize the Fe_3O_4 nanoparticles (NPs) and CMC–Fe_3O_4 beads. X-ray diffraction (XRD) patterns were recorded on a Siemens D5000 diffractometer with Cu Kα radiation (λ = 1.5418 Å) to identify their crystal structures. Transmission electron microscopy images were taken on a Philips CM200 TEM to investigate the morphology of the Fe_3O_4 NPs. The BET specific surface area (SSA), the N_2 adsorption and desorption isotherms, the BJH total pore volume and pore size distribution were determined using a TriStar 3000 V6. 07 A (serial number 2134) surface area analyzer at 77 K. For surface chemical composition investigation of Fe_3O_4 NPs, we used two X-ray photoelectron spectroscopy units, one (Thermo Fisher Scientific K Alpha) using an Al Kα source (1486.7 eV) and the other (ESCALAB 3 MKII de VG) using a Mg Kα source (1253.6 eV) to collect high resolution scans of the carbon C1s, oxygen O1s, and iron Fe2p elements. Details about the XPS experimental conditions and spectra curve fitting are given in the Supporting Information section. To further understand the role of CMC in the CMC Fe_3O_4 beads, scanning electron microscopy (Hitachi S-4700 field emission-scanning transmission electron microscopy) images of the CMC–Fe_3O_4 beads were collected.

Adsorption Mechanisms

Adsorption isotherms were measured for toluene onto Fe_3O_4 NPs and CMC–Fe_3O_4 beads by incremental injection of toluene into reference and treatment flasks, with the latter containing 0.1020 ± 0.0002 g of Fe_3O_4 NPs or $1 \pm 2 \times 10^{-4}$ g of Fe_3O_4–CMC beads (i.e., to expose comparable surface areas). We plotted the amount of toluene adsorbed per gram of Fe_3O_4 NPs as a function of toluene remaining in the gas phase and fitted the data using the multi site Langmuir model reported by Konda et al.(23) Details about the fitting are given in the Supporting Information.

Adsorbents Synthesis

The Fe_3O_4 NPs were synthesized by coprecipitating a 2:1 solution of $FeCl_3 \cdot 6H_2O$ and $FeCl_2 \cdot 4H_2O$ with ammonium hydroxide in deoxygenated water at 85 °C as described by Massart.(19) We recycled the Fe_3O_4 NPs after VOC adsorption experiments by collecting them on a magnetic retriever and placing them overnight in an air ventilated oven at 50 °C. We recycled each batch of Fe_3O_4 NPs three times. The carboxymethyl cellulose-magnetite beads (CMC–Fe_3O_4 beads) were prepared on the basis of the method described by and Luo.(24) Briefly, dried Fe_3O_4 NPs were added to a solution of carboxymethyl cellulose in water in the ratio of 1:2:5 (Fe_3O_4 NPs:CMC:H_2O by weight). The resulting mixture was added dropwise to a regenerating aqueous solution of 0.2 M $FeCl_2$. The resulting beads were collected with a magnetic retriever and dried in an air ventilated oven at 50 °C.

Gas Mixtures

Separate and diluted stock mixtures of each compound (BTEX) were freshly prepared and left to equilibrate for 2 h before use in experiments. Details on the preparation of stock mixtures are given in the Supporting Information section.

Removal Efficiency and Byproduct Analysis

VOCs removal efficiencies and adsorption isotherms were determined by monitoring the gas phase concentration of different VOCs in air exposed to the Fe_3O_4 adsorbents. The concentration of VOCs present in the reaction chamber was determined by preconcentrating the VOCs on a CARBOXEN/polydimethylsiloxane (CAR/PDMS) solid phase microextraction (SPME) fiber,(25) which was desorbed in a gas chromatograph equipped with a flame ionization detector (GC–FID). To investigate the presence of any byproduct that may have formed during the adsorption process, divinylbenzene/polydimethylsiloxane (DVB/PDMS) and CAR/PDMS fibers were deployed for sample collection whereas desorption was performed using a gas chromatograph coupled with a mass spectrometer (GC–MS). Experimental details are given in the Supporting Information section.

We measured the removal efficiency of Fe_3O_4 NPs for each individual BTEX compound using a static set up. The experiments involved injecting one of the selected BTEX compound to make up a 100 ppmv mixing ratio (1 ppmv ~2.45×10^{13} molecules cm^{-3} at STP) in two flasks: one containing $4 \pm 2 \times 10^{-4}$ g of Fe_3O_4 NPs (treated flask) and one without Fe_3O_4 NPs (reference flask) then comparing the gas phase mixing ratio of the BTEX compound for the treatment and the reference flasks using eq 1. Reference and treated flasks were systematically evacuated, flushed with nitrogen at least three times, and analyzed by GC-FID before injecting any of the BTEX compounds.

For Fe_3O_4–CMC beads, we used a diaphragm pump (KNF Neuberger Inc. 609/890-8600) to circulate 2 L/min of air into which toluene was injected making up a mixing ratio of 100 ppmv. We used a two-way valve to first bypass the airstream around the adsorbent column at which point sampling was carried out to obtain a reference value for untreated air. Then the valve was turned to direct the air containing the toluene through $3.2 \pm 2.0 \times 10^{-4}$ g of CMC–Fe_3O_4 beads packed in a 10 cm long with a diameter of 1 cm glass column.

For the static and dynamic systems described above, the removal efficiency was calculated from peak areas (PA) in the chromatograms as a relative measurement following eq 1:

$$removal\ efficiency = \left(\frac{PA_{reference} - PA_{treated}}{PA_{reference}}\right) \times 100 \qquad (1)$$

where $PA_{reference}$ and $PA_{treated}$ are directly proportional to the concentrations of the selected compound in the reference and the treated flasks, respectively. At least three replicate tests were carried out per compound.

Materials and Supplies

Iron salts, $FeCl_3 \cdot 6H_2O$ (>98%) and $FeCl_2 \cdot 4H_2O$ (≥99%), and low viscosity carboxymethylcellulose (CAS 9004-32-4) were purchased from Sigma Aldrich and used as received. Benzene (>99%), toluene (99.8%), *o*-xylene (96%), and $NH_3 \cdot H_2O$ (≥25% ammonia, NH_3) were all purchased from Fisher Scientific and ethylbenzene (99%) from Anachemia. Ultra high purity nitrogen (99.999%) was purchased from MEGS Specialty Gases and extra dry compressed air (Content of O_2 19.5–23.5% and H_2O < 10 ppm) was purchased from Praxair. The SPME fibers were purchased from Sigma-Aldrich and conditioned as suggested by the manufacturer.

Results and Discussion

Characterization of the Adsorbents

The XRD relative peak intensities of the synthesized Fe_3O_4 NPs and CMC–Fe_3O_4 beads matched those of reference Fe_3O_4 (according to the JCPDS card # 19-0629) as shown in Figure 1a,d. The average Scherrer size of the Fe_3O_4 NPs and the unit cell value were 7.5 and 0.821 nm, respectively. The unit cell value is much smaller than those of both stoichiometric magnetite (0.839 nm) and maghemite (0.834 nm);(18) there are two reasons that can explain this difference. One is related to the small size of the nanoparticles where high surface energies at the surface cause a contraction in the crystal resulting in a smaller parameter.(26) Another possibility is that the surface layer contains vacancies, which are also reported to cause a decreases in unit cell parameters(27) and could be present if Fe_3O_4 had oxidized to γ-Fe_2O_3.(26) We provide details about structural identification in the Supporting Information section. The XPS spectra in Figure 4 showed components of the $Fe2p_{3/2}$ peak assigned to Fe^{2+} (octahedral) and its satellite at binding energies (BE) of 710.8 ± 0.2 eV and 716.8 ± 0.2 eV, respectively and those of Fe^{3+} (octahedral), Fe^{3+} (tetrahedral), and Fe^{3+} satellite at 711.4 ± 0.2, 713.5 ± 0.2, and 720.2 ± 0.2 eV,

respectively. On the O1s spectrum, the main oxide peak (O–Fe) was assigned at 530.7 ± 0.2 eV and is shown in Figure 5. Our values are all slightly higher than those reported by Poulin et al.(28) for stoichiometric Fe_3O_4. There are two reasons to explain the higher binding energies. The first relates to the small size of the nanoparticles.(29) The values obtained by Poulin et al.(28) were reported for NPs of 86 nm, which is over 4 times larger than our NPs and may explain the observed higher binding energies.(29) The other reason relates to the formation of an oxidized surface layer because the binding energies resemble the values for γ-Fe_2O_3.(28) This could be anticipated because Fe_3O_4 readily oxidizes to γ-Fe_2O_3 in air.(18) In addition, the formation of an oxidized layer of γ-Fe_2O_3 with more Fe^{3+} relative to Fe^{2+} would result in the formation of cation vacancies,(18) which is consistent with the smaller lattice parameter obtained by XRD. The presence of Fe^{2+} and its satellite peak as observed in the XPS spectra in Figure 4 suggests the iron oxide nanoparticles are composed of Fe_3O_4 with an oxidized layer of γ-Fe_2O_3 at the surface. The TEM images confirm the crystallinity of the Fe_3O_4 NPs and show a large distribution of sizes ranging from 5 to 20 nm as seen in Figure 2a, which also confirm the unit cell values obtained by XRD. The specific surface area (SSA) of Fe_3O_4 NPs and CMC–Fe_3O_4 beads were 77 ± 7 and 16 ± 6 m^2/g, respectively as presented in Table 1. Note that the surface area of plain CMC in the beads was below 1 m^2 and could not be measured by the instrument. Therefore, the observed SSA of CMC–Fe_3O_4 beads can be attributed to the Fe_3O_4 NPs only. Furthermore, SEM images of CMC–Fe_3O_4 beads in Figure 6 show a dense and smooth material exempt of crystallinity and porosity suggesting that CMC acts as a nonporous binder holding the nanoparticles together and possibly encapsulating them, which can explain the reduced SSA and pore volumes relative to the bare Fe_3O_4 NPs. The N_2 BET adsorption and desorption profiles presented in Figure 3a,c show that the isotherms corresponded to a type IV in the Langmuir classification.(30) The porosity volumes of Fe_3O_4 NPs and CMC–Fe_3O_4 beads as a function of pore size distribution are shown in Figure 3b,d. The average BJH pore size was 10 ± 3 nm, revealing that most of the pore volume was associated with the mesoporosity of the adsorbents.(31)

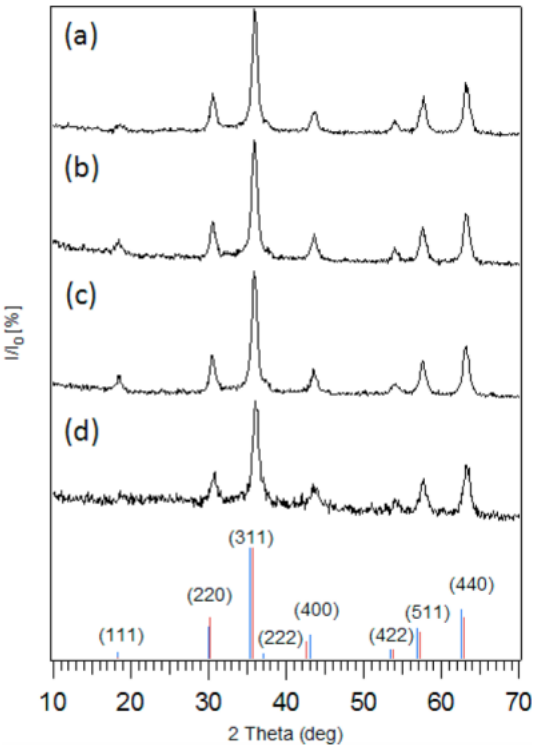

Figure 1. X-ray diffraction patterns of (a) fresh Fe_3O_4 NPs (b) cycle 1 Fe_3O_4 NPs (c) cycle 2 Fe_3O_4 NPs, and (d) CMC–Fe_3O_4 beads. The blue and red sticks represent standard Fe_3O_4 and γ-Fe_2O_3, respectively.

Adsorption Mechanisms

The mechanism by which aromatics adsorb onto the Fe_3O_4 NPs was studied by monitoring the adsorption capacity of toluene, used herein as a model compound, by the Fe_3O_4 NPs, bare and within the CMC matrix (CMC–Fe_3O_4 beads), as a function of toluene equilibrium pressure. The adsorption isotherm for the gaseous toluene–Fe_3O_4 NPs system displayed defined multiple steps over the relative pressure range as depicted in Figure 7a. Although we cannot unequivocally suggest a definite mechanism, the multiple steps could correspond to different

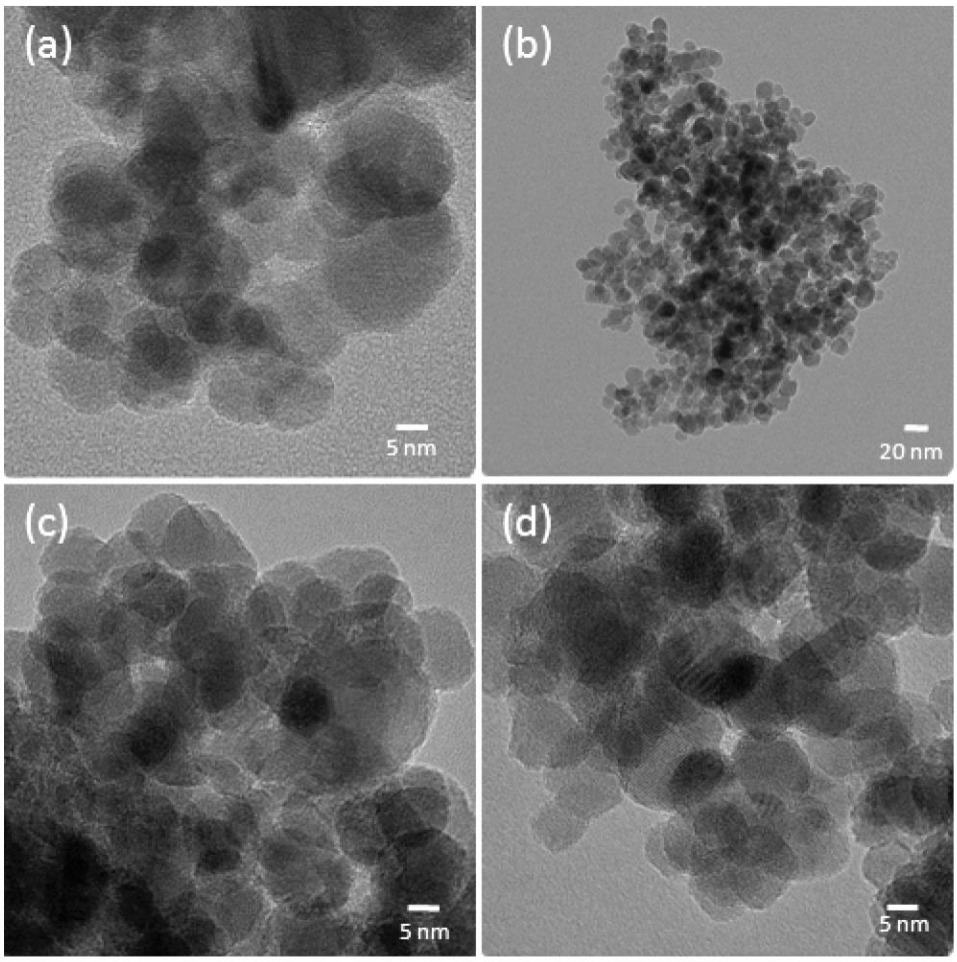

Figure 2. TEM images of (a) and (b) fresh Fe_3O_4 NPs, (c) Fe_3O_4 NPs regenerated once, and (d) Fe_3O_4 NPs regenerated twice.

adsorption regions, which can result from heterogeneity due to differing functional groups, atoms, or impurities.(32) The multiple steps (Figure 7a) can arise from the interaction between Fe^{2+} and Fe^{3+} (Figure 4) with the π electrons groups of toluene. The interaction of aromatics and transition metal oxide has been described in terms of acid base chemistry, where the delocalized π electrons of the aromatic ring of toluene are capable of sharing electron density (basic character) through σ bonding with the unfilled 3d metal orbital of the iron cations (acidic character).(3, 33) The back-donation of electron density from the filled metal orbitals to the unfilled orbitals of toluene has also been suggested.(3)

For the CMC–Fe_3O_4 beads, we observe in Figure 7b a less pronounced stepwise increase and an overall decrease in the adsorption capacity in Table 2 from the values of a1–a4. The reduced adsorption capacity can be explained by two reasons. First, the reduced values in the CMC–Fe_3O_4 beads' total pore volume and BET specific surface area (Figure 3b and Table 1) result in less adsorption sites. Second, the composite of CMC–Fe_3O_4 beads results in reduced Fe^{2+} and Fe^{3+} availability due to binding with the carboxylate groups of CMC.(34) Our hypothesis is that

there is a coupled influence between chemical and geometrical heterogeneities of the Fe_3O_4 NPs, bare and within the CMC matrix, resulting in the different adsorption regions in the isotherms in Figure 7a,b.

In the literature, multiple steps of isotherms are associated with multilayer formation. Giles et al.(35) associated a plateau with the saturation of one layer by adsorbate molecules. They have also explained that after saturation of a layer, molecules can reorient themselves providing "new" sites for adsorption. Joseph et al.(3) reported that as coverage increased, the adsorbate–adsorbate interactions dominated and induced a change in the adsorption geometry from a flat-like to tilted configuration. The steps could also correspond to capillary condensation, which is characteristic of adsorption on mesoporous adsorbents.(35, 36) An estimate of surface coverage, however, assuming a flat like configuration and a cross sectional area of 0.473 nm^2 for toluene,(37) reveals that approximately 0.08 m^2 of 0.8 m^2 the surface was covered and the saturation capacity was not reached. One may speculate then that these steps correspond to active sites of different energies potentially related to Fe^{2+}, Fe^{3+}, and or structural vacancies in the nanoparticles rather than multilayer formation. Another potential explanation of our observation is that the adsorption of toluene is modifying properties such as magnetism of the nanoparticles. We did not study the influence of magnetism on the adsorption of toluene, but it has been shown that gas adsorption decreased the magnetization of materials.(38, 39) If magnetism has an effect on adsorption as well, it is possible that decreases in magnetism occurring with increasing coverage may change the surface energy of the sites and result in those steps. Further investigations are needed to determine whether magnetism affects adsorption at the molecular level.

We accounted for the multiple steps in the adsorption isotherm quantitatively. Models for multilayer adsorption such as GAB, which considers adsorbent–adsorbate interactions, were unsuccessful, whereas models involving summation of local isotherms and energy distribution functions involved several unknown parameters precluding us to obtain accurate estimates.(32, 36) Therefore, we fitted the adsorption isotherm on the basis of the mathematical model described by Konda et al.,(23) where multistep isotherms are described as a sum of individual Langmuir adsorptions resulting from energetically heterogeneous sites and interactions between the adsorbed molecules. Thus, they associate each step to a type of adsorption mechanism. The overall equation is described by eq 2:

$$q_i = \sum_{i=1}^{s} \frac{a_i k_i [(c - b_i) + abs(c - b_i)]}{2 + k_i [(c - b_i) + abs(c - b_i)]} \quad (2)$$

where *a* accounts for the monolayer adsorption capacity, *b* represents the limiting concentration after which a subsequent adsorption mechanism begins, and *k* is the adsorption equilibrium constant for a given step *i*. We found the best fit for the adsorption of gaseous toluene onto Fe_3O_4 NPs for $i = 4$ (Figure 7a). We applied the same equation for the adsorption of toluene onto CMC–Fe_3O_4 beads (Figure 7b). The fits and calculated residuals are plotted in

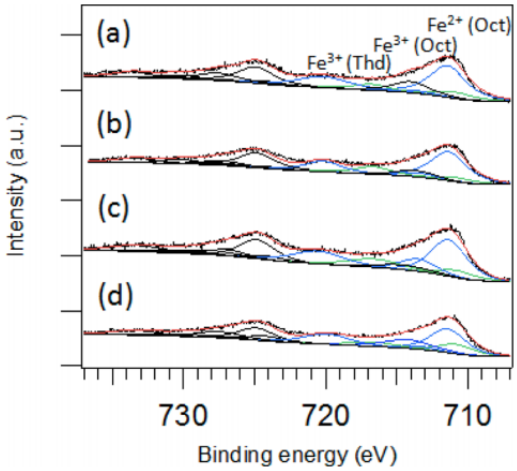

Figure 4. XPS for Fe2p (top) of Fe_3O_4 NPs exposed to (a) 0, (b) 300, (c) 900, and (d) 2790 ppmv of toluene. The outermost red and black lines represent the actual and fitted spectra, respectively.

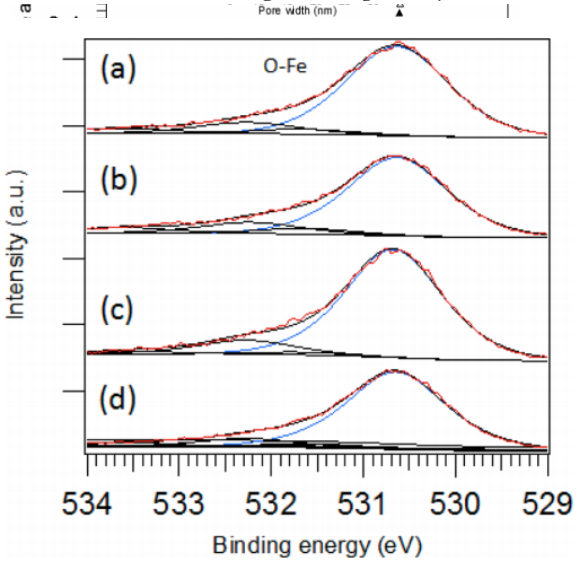

Figure 5. XPS for O1s of Fe_3O_4 NPs exposed to (a) 0, (b) 300, (c) 900, and (d) 2790 ppmv of toluene. The outermost red and black lines represent the actual and fitted spectra, respectively.

Figure 7a,b as dotted lines and the calculated parameter values are given in Table 2. We calculated the total adsorption capacity by adding individual "a_i", which totalled 12×10^{-8} and 2.9×10^{-8} mol/g for the CMC–Fe_3O_4 beads and Fe_3O_4 NPs, respectively. By comparing the parameters for both adsorbents, we found that the k_1 and k_4 values for both unsupported and supported NPs were comparable within 5%. We suggest that k_1 and k_4 reflect chemical interactions that can occur between iron cation sites in Fe_3O_4 NPs and delocalized pi electrons of toluene.(3, 18) We found that values of k_2 and k_3 were significantly lower for the CMC–Fe_3O_4 beads comparing with those of the bare Fe_3O_4 NPs. We suspect that the reduced k_2 and k_3 values reflect the adsorption

mechanisms influenced by pore volume and surface areas, which are both reduced for CMC–Fe_3O_4 beads. Further investigation on the adsorption energies of each region and the molecular level interactions will enable the development of more effective adsorbents; namely, tailoring the chemical and physical features of an adsorbent to target specific compounds for the treatment of polluted air.

Magnetite Redox Activity

We examined the change in the Fe^{2+}/ Fe^{3+} ratio on the surface of the Fe_3O_4 NPs when subjected to toluene to determine whether the surface layer was catalytically active. From the deconvoluted XPS peaks in the $Fe2p_{3/2}$ (Figure 4), we calculated the ratios of Fe^{2+}/ Fe^{3+} and plotted them as a function of increasing concentrations of toluene vapor (Figure 8). It is evident that at concentrations of toluene above 300 ppmv, the Fe^{2+}/ Fe^{3+} ratio increases, corresponding to a reduction of the surface layer of the Fe_3O_4 NPs. The differences in the extent of oxidation for the three data sets can be due to the small size and the polydispersity of the Fe_3O_4 NPs as observed by TEM in Figure 2. The effect of decreased size on the increased oxidation has been reported(8) and could result in different oxidation capacity (i.e., lower ratio of Fe^{2+}/Fe^{3+}). At this stage, we are unable to confirm the exact mechanism(s) to explain the reduction of the surface layer under our experimental conditions; we can merely postulate on a mechanism involving a reductive adsorption, where the toluene is oxidized and the iron is reduced, only at relatively elevated toluene concentrations. The pathways to the oxidation of toluene could proceed by CH_3 hydrogen abstraction as reported for a similar system ethylbenzene(3) or it could occur through the breaking of the benzene ring.(40) Because the substituent of ethyl benzene or *o*-xylene is also electron donating,(33) we believe these compounds also potentially cause redox changes on magnetite nanoparticles at higher concentrations. In addition, the small size of the nanoparticle (10 nm) could be driving the catalytic activity at those conditions due to higher surface energies. At this scale, it has been shown that divalent iron cations were more stable than trivalent cations.(7) Therefore, the catalytic activity of the nanoparticle observed in Figure 8 could be driven by the decrease in excess surface energy on going from the trivalent oxide (oxidized layer) to the reduced form of divalent cations.

Table 1. Removal Efficiencies of BTEX[a] with Fe_3O_4 NPs and CMC−Fe_3O_4 Beads

adsorbent	surface area [$m^2 \cdot g^{-1}$]	pollutant (100 ppmv)	removal efficiency [%]	temperature [°C]	relative humidity [%]	reusability
			Batch Experiments			
Fe_3O_4 NPs						
fresh	77 ± 7	benzene	83 ± 8	25	0 (dry air)	
		toluene	95 ± 5			
		ethylbenzene	97 ± 1			
		o-xylene	98 ± 2			
cycle 1	70 ± 7	toluene	99	25	0 (dry air)	100% of original performance (3 cycles)
cycle 2			92			
cycle 3			98			
average			96 ± 4			
			Flow Experiments			
CMC-Fe_3O_4 beads	16 ± 6	toluene	83 ± 10	25	0 (dry air)	N/A

[a]BTEX corresponds to benzene, toluene, ethylbenzene, and *o*-xylene at mixing ratios of 100 ppmv.

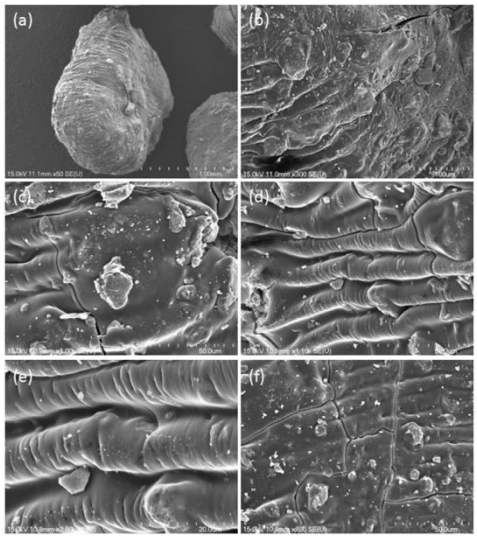

Figure 6. SEM images of CMC−Fe_3O_4 beads.

It is possible that humidity can impact the catalytic effect at the surface of the NPs as H_2O is known to dissociate on Fe_3O_4 NPs.(5) The dissociated H_2O would appear as surface OH at 532 ± 0.2 eV in the O1s spectrum in Figure 5. However, we did not observe in Figure 5 any trend in the OH peak with varying toluene concentration, so we do not believe those surface hydroxyls, which could be coming from dissociated water, were involved in the potential oxidation of toluene and reduction of Fe^{3+}. The influence of water vapor on adsorption of toluene and benzene onto FeO, a related oxide, has been shown to depend on surface coverage.(6) It has also been shown that humidity influences the uptake of gases and reactions onto related iron oxides in the atmosphere.(41) Therefore, it is possible that under different conditions, humidity play a role on the adsorption of BTEX and reactions on Fe_3O_4 NPs.

Removal Efficiencies and Byproduct Analysis

One of our main goals was to assess the potential for Fe_3O_4 NPs to be used as an air remediation medium to reduce the emissions of VOCs by measuring the removal efficiency for an array of gas phase aromatic compounds (BTEX). We found that at room temperature (25 ± 3 °C), separate mixtures of 100 ppmv of benzene, toluene, ethylbenzene and *o*-xylene, were reduced by 83 ± 7%, 95 ± 5%, 97 ± 2%, and 98 ± 1%, respectively, after being exposed to 4 ± 2 × 10^{-4} g of Fe_3O_4 NPs (Table 1). Our results demonstrate that under our laboratory conditions, Fe_3O_4 NPs can remove BTEX with efficiencies that compare well with conventional adsorbents, activated carbon and zeolite, for which the removal efficiencies are reported to range from 80 to 96% and 94 to 98%, respectively.(42, 43)

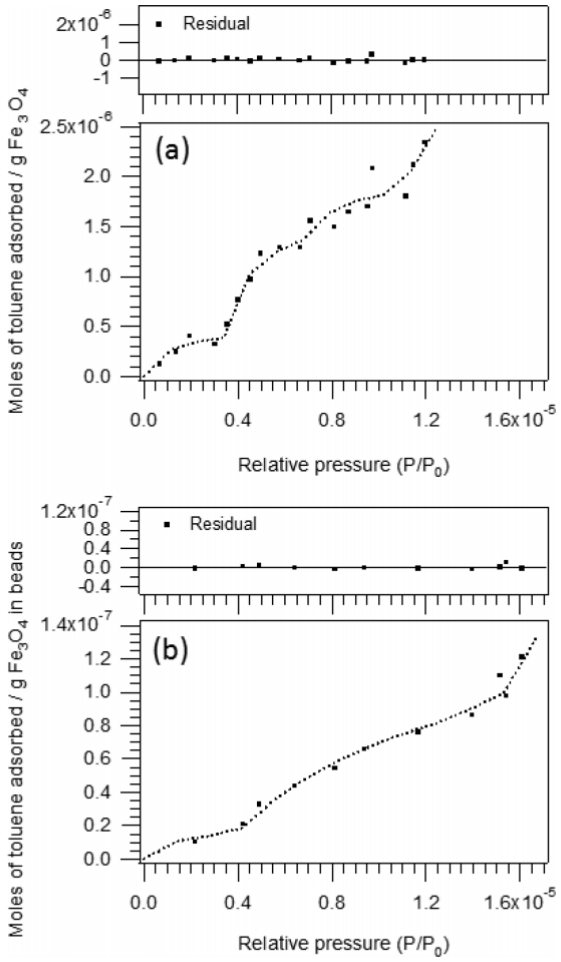

Figure 7. Experimental (large squares) and fitted (small squares) adsorption isotherms of toluene on (a) Fe_3O_4 NPs and (b) CMC–Fe_3O_4 beads.

An adsorbent that can be recycled and reused with minimal reduction in its performance is essential for a practical application in the field of pollution remediation. After three cycles of using and recycling the Fe_3O_4 NPs, we found the average removal efficiency to be 96 ± 4% for 100 ppmv toluene (used as a model for BTEX) (Table 1), which demonstrates that recycled Fe_3O_4 NPs performed as efficiently as fresh ones at experimental conditions. Note that the recycling capacity is applicable for concentrations below 300 ppmv, which is a conservative upper limit when compared with levels of BTEX observed in ambient air of heavily polluted cities. For ambient air levels of toluene measured in various sites, Gilli et al.(44) reported concentrations of 17 ppbv(44) in Turin, Italy, and Niu et al.(45) recently reported concentrations of 110 ppbv in industrial areas in China (1 ppmv = 3.75 mg·m^{-3}).

Furthermore, we studied the effect of regeneration on the physical and chemical properties of the adsorbent to test the durability of the Fe_3O_4 NPs and to investigate the mechanisms of VOC removal. We did not detect changes after regeneration in the relative intensities and positions of peaks in the XRD patterns of regenerated NPs, which indicates that the recycling process did not cause any structural damage to the adsorbent (Figure 1). We also found that the specific surface area of the regenerated NPs was within the experimental error with respect to the freshly made NPs (Table 1). We also did not detect any size or shape changes from TEM images (Figure 2). As depicted in Table 1 and Figures 1 and 2, physical and chemical integrities of the Fe_3O_4 NPs were retained after the recycling procedure, which suggests a cycling process of adsorption and desorption for the continuous removal of BTEX is conceivable. It is noteworthy that there are several ways for the regeneration of magnetic nanoparticles besides those deployed in this study such as induced heating of the NPs in an alternate magnetic field(46) or electrochemistry.(47)

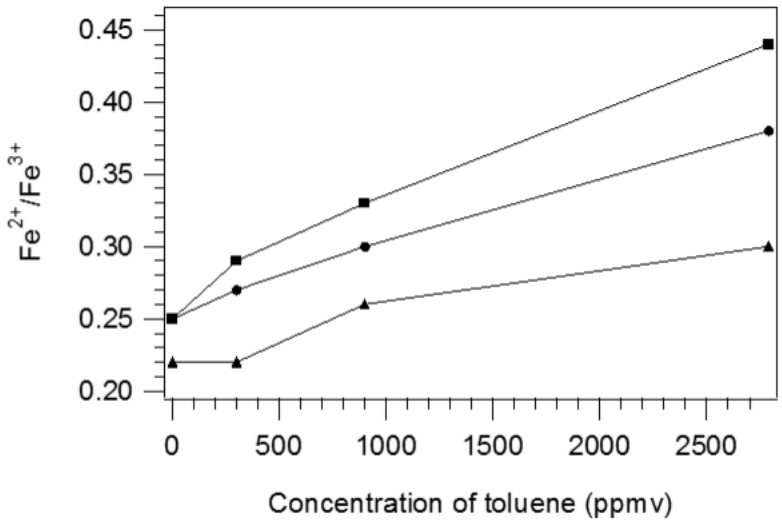

Figure 8. Changes in the Fe^{2+}/Fe^{3+} ratio as a function of increasing toluene concentration (the lines are used to guide the eye). The circles correspond to analysis at the McGill facility, and the squares and triangles correspond to analyses carried out at the Polytechnique facility.

We verified that the process of BTEX removal was predominantly due to adsorption by analyzing for other gaseous compounds such as aldehydes and aromatics, which could be released as a result of undesired oxidation reactions at the adsorbent surface or from secondary reactions during the adsorption of toluene. We performed 8 h long experiments during which we used SPME to sample air from the gastight reaction chamber; no other aromatics and no aldehydes were detected by GC–MS for which the detection limit is typically 10^{-1} ng/mL.(48) From this, we conclude that the interaction of toluene and Fe_3O_4 NPs does not result in the formation of gaseous byproduct. Studies show that Fe_3O_4 NPs is catalytically inactive when exposed to ethylbenzene, which has similar chemically reactivity to toluene by virtue of its π-electrons ring.(3) However, another possibility is that byproduct are formed but adsorbed by the NPs. Nonetheless, we did not observe any change in the Fe^{2+}/Fe^{3+} in Fe_3O_4 NPs when exposed to toluene concentrations below 300 ppmv, suggesting no byproduct resulting from redox reactions were formed. Therefore, Fe_3O_4 NPs are promising for the treatment of polluted air under similar conditions, i.e., at room temperature (25 ± 3 °C). Further studies over a wide range of temperatures and pressures are desired to ensure the benign nature of Fe_3O_4 NPs for BTEX remediation from atmospheric matrices.

In practical scenarios, if NPs are used for remediation, the concern about their dispersion in air, which would have detrimental impacts on health(49) and the environment,(50) must be taken into account. To this end, we used carboxymethyl cellulose (CMC) as a support to bind the Fe_3O_4 NPs. We found that Fe_3O_4 NPs fixed on CMC subjected to air flows of 2 and 30 L/min did not suffer any weight loss outside the experimental errors of the analytical balances used (± 2.0×10^{-4} g and ±0.02 g, respectively). By visual inspection, no NPs were observed

outside the sample cell indicating they were strongly bound by the CMC. We also found that at 2 L/min, $3.2 \pm 2.0 \times 10^{-4}$ g of CMC–Fe_3O_4 reduced 100 ppmv of gas phase toluene by 83 ± 14%. Note that the adsorption capacity was found to be lower as compared to the bare Fe_3O_4 NPs (Figure 7b) and that we did not observe any adsorption of toluene on bare CMC particles in the absence of Fe_3O_4 NPs. Nevertheless, with CMC as a support, the Fe_3O_4 NPs were used as millimeter sized clusters, which facilitated their separation from the system. We believe that using a larger sized cluster would allow mechanical filtration rendering this technique attractive for a wide range of applications such as indoor air circulation systems.

Table 2. Calculated Parameters from the Adsorption Isotherms of Toluene on Fe_3O_4 NPs and CMC−Fe_3O_4 Beads

adsorbent	a_1 (10^{-7})	a_2 (10^{-6})	a_3 (10^{-7})	a_4 (10^{-6})	b_2 (10^{-6})	b_3 (10^{-6})	b_4 (10^{-5})	k_1 (10^{+5})	k_2 (10^{+6})	k_3 (10^{+5})	k_4 (10^{+5})
Fe_3O_4 NPs	3.8	1	5	1	2.8	6.8	1.12	9.3	1.9	8.2	5.5
CMC−Fe_3O_4 beads	0.2	0.04	0.22	0.04	4	13	1.53	9.3	0.1	0.09	5.8

Conclusion

Our findings show that BTEX adsorb efficiently to Fe_3O_4 NPs at room temperature and pressure in air. During this process no gas phase byproduct or bulk structural changes were detected. Because higher concentrations of toluene (i.e., >300 ppmv) resulted in redox changes in the Fe_3O_4 NPs, the applicability would be limited to lower concentration settings (<100 ppmv) of toluene and other BTEX such as those encountered in indoor air. Further studies investigating the removal efficiency at other conditions are needed to identify their applicability to real systems. With respect to practicality, the efficiency of the composites of CMC–Fe_3O_4 NPs to adsorb toluene could be improved by changing the synthesis technique to include blowing agents to create pores or by using cellulosic supports displaying high surface areas such as cellulose fibers. Using natural and widely accessible materials such as Fe_3O_4 NPs and cellulosic materials would save costs to the environment with respect to energy efficiency and reduction of wastes and aid in the global efforts dedicated to the reduction of air pollution for the protection of public health and the environment in both developed and developing countries.

Supporting information

Experimental details for the determination of the removal efficiency (RE%), adsorption isotherm, stock gas mixture preparation, and byproduct analysis using GC–FID and GC–MS, X-ray photoelectron spectroscopy (Table S1) and X-ray diffraction (Table S2) characterization. This information is available free of charge via the Internet at http://pubs.acs.org/.

Author Information

Corresponding Author

Parisa A. Ariya - *†Department of Chemistry and ‡Department of Atmospheric and Oceanic Sciences, McGill University, 801 Sherbrooke West, Montreal, QC, Canada H3A 2K6*; Email: parisa.ariya@mcgill.ca

Author

Nermin A. Eltouny - *†Department of Chemistry and ‡Department of Atmospheric and Oceanic Sciences, McGill University, 801 Sherbrooke West, Montreal, QC, Canada H3A 2K6*

Notes

The authors declare no competing financial interest.

Acknowledgment

We are very grateful to Dr. J. Lefebvre for contributing to the collection and analysis of XPS spectra. We thank Prof. Haghighat and Dr. Lee at the Department of Building, Civil, and Environmental Engineering at Concordia University for making their setup available to us. We acknowledge NSERC, CFI, FQRNT, and Environment Canada for their financial support. We sincerely thank Dr. M. Subir, Mr. C. Wilde, and Dr. D. Deeds for making valuable comments to improve this manuscript. We extend our gratitude to the reviewers for providing constructive comments to help improve the manuscript.

References

(1) Laurent, S.; Forge, D.; Port, M.; Roch, A.; Robic, C.; Vander Elst, L.; Muller, R. N. Magnetic Iron Oxide Nanoparticles: Synthesis, Stabilization, Vectorization, Physicochemical Characterizations, and Biological Applications. *Chem. Rev.* 2008, *108*, 2064−2110.

(2) Mayo, J. T.; Yavuz, C.; Yean, S.; Cong, L.; Shipley, H.; Yu, W.; Falkner, J.; Kan, A.; Tomson, M.; Colvin, V. L. The effect of nanocrystalline magnetite size on arsenic removal. *Sci. Technol. Adv. Mater.* 2007, *8*, 71.

(3) Joseph, Y.; Wuhn, M.; Niklewski, A.; Ranke, W.; Weiss, W.; Woll, C.; Schlogl, R. Interaction of ethylbenzene and styrene with iron oxide model catalyst films at low coverages: A NEXAFS study. *Phys. Chem. Chem. Phys.* 2000, *2*, 5314−5319.

(4) Udovic, T. J.; Dumesic, J. A. Adsorptive properties of magnetite surfaces as studied by temperature-programmed desorption: Studies of O2, NO, CO2, and CO adsorption. *J. Catal.* 1984, *89*, 314−326.

(5) Joseph, Y.; Ranke, W.; Weiss, W. Water on FeO(111) and Fe3O4(111): Adsorption Behavior on Different Surface Terminations. *J. Phys. Chem. B* 2000, *104*, 3224−3236.

(6) Nakazawa, M.; Somorjai, G. A. Coadsorption of water and selected aromatic molecules to model the adhesion of epoxy resins on hydrated surfaces of zinc oxide and iron oxide. *Appl. Surf. Sci.* 1995, *84*, 309−323.

(7) Navrotsky, A.; Ma, C.; Lilova, K.; Birkner, N. Nanophase Transition Metal Oxides Show Large Thermodynamically Driven Shifts in Oxidation-Reduction Equilibria. *Science* 2010, *330*, 199−201.

(8) Santoyo Salazar, J.; Perez, L.; de Abril, O.; Truong Phuoc, L.; Ihiawakrim, D.; Vazquez, M.; Greneche, J.-M.; Begin-Colin, S.; Pourroy, G. Magnetic Iron Oxide Nanoparticles in 10−40 nm Range: Composition in Terms of Magnetite/Maghemite Ratio and Effect on the Magnetic Properties. *Chem. Mater.* 2011, *23*, 1379−1386.

(9) Seinfeld, J. H.; Pandis, S. N. *Atmospheric chemistry and physics from air pollution to climate change*; J. Wiley: Hoboken, NJ, 2006.

(10) Koppmann, R. *Volatile organic compounds in the atmosphere*; Blackwell Publishers: Oxford, U.K.; Ames, IA, 2007.

(11) Kacew, S.; Lemaire, I. Recent Developments in Benzene Risk Assessment. *J. Toxicol. Environ. Health A* 2000, *61*, 485−498.

(12) Bruinen de Bruin, Y.; Koistinen, K.; Kephalopoulos, S.; Geiss, O.; Tirendi, S.; Kotzias, D. Characterisation of urban inhalation exposures to benzene, formaldehyde and acetaldehyde in the European Union. *Environ. Sci. Pollut. Res.* 2008, *15*, 417−430.

(13) Zhou, Y.; Zhang, H.; Parikh, H. M.; Chen, E. H.; Rattanavaraha, W.; Rosen, E. P.; Wang, W.; Kamens, R. M. Secondary organic aerosol formation from xylenes and mixtures of toluene and xylenes in an atmospheric urban hydrocarbon mixture: Water and particle seed effects (II). *Atmos. Environ.* 2011, *45*, 3882−3890.

(14) Parmar, G. R.; Rao, N. N. Emerging Control Technologies for Volatile Organic Compounds. *Crit. Rev. Environ. Sci. Technol.* 2009, *39*, 41−78.

(15) Yang, R. T. *Adsorbents: fundamentals and applications*; Wiley-Interscience: Hoboken, NJ, 2003.

(16) Jaroniec, M. Design, Synthesis, and Characterization of Ordered Mesoporous Materials for Environmental Applications. In *Combined and Hybrid Adsorbents*; Loureiro, J., Kartel, M., Eds.; Springer: Netherlands, 2006; Vol. *16*, pp 23−36.

(17) Plata, D. e. L.; Hart, A. J.; Reddy, C. M.; Gschwend, P. M. Early Evaluation of Potential Environmental Impacts of Carbon Nanotube Synthesis by Chemical Vapor Deposition. *Environ. Sci. Technol.* 2009,

43, 8367−8373.

(18) Cornell, R. M.; Schwertmann, U. *The iron oxides: structure, properties, reactions, occurrences, and uses*; Wiley-VCH: Weinheim, 2003.

(19) Massart, R. Preparation of aqueous magnetic liquids in alkaline and acidic media. *IEEE Trans. Magn.* 1981, *17*, 1247−1248.

(20) Chowdhury, S. R.; Yanful, E. K. Arsenic and chromium removal by mixed magnetite-maghemite nanoparticles and the effect of phosphate on removal. *J. Environ. Manag.* 2010, *91*, 2238−2247.

(21) Wang, Y.; Morin, G.; Ona-Nguema, G.; Juillot, F.; Calas, G.; Brown, G. E. Distinctive Arsenic(V) Trapping Modes by Magnetite Nanoparticles Induced by Different Sorption Processes. *Environ. Sci. Technol.* 2011, *45*, 7258−7266.

(22) Gorski, C. A.; Scherer, M. M. Influence of Magnetite Stoichiometry on FeII Uptake and Nitrobenzene Reduction. *Environ. Sci. Technol.* 2009, *43*, 3675−3680.

(23) Konda, L. N.; Czinkota, I.; Füleky, G.; Morovjan, G. Modeling of Single-Step and Multistep Adsorption Isotherms of Organic Pesticides on Soil. *J. Agric. Food Chem.* 2002, *50*, 7326−7331.

(24) Luo, X.; Zhang, L. High effective adsorption of organic dyes on magnetic cellulose beads entrapping activated carbon. *J. Hazard. Mater.* 2009, *171*, 340−347.

(25) Koziel, J. A.; Pawliszyn, J. Air sampling and analysis of volatile organic compounds with solid phase microextraction. *J. Air Waste Manag. Assoc.* 2001, *2*, 173−184.

(26) Qi, W. H.; Wang, M. P.; Su, Y. C. Size effect on the lattice parameters of nanoparticles. *J. Mater. Sci. Lett.* 2002, *21*, 877−878.

(27) Yang, J. B.; Zhou, X. D.; Yelon, W. B.; James, W. J.; Cai, Q.; Gopalakrishnan, K. V.; Malik, S. K.; Sun, X. C.; Nikles, D. E. Magnetic and structural studies of the Verwey transition in Fe[sub 3 - delta]O[sub 4] nanoparticles. *J. Appl. Phys.* 2004, *95*, 7540−7542.

(28) Poulin, S.; França, R.; Moreau-Bélanger, L.; Sacher, E. Confirmation of X-ray Photoelectron Spectroscopy Peak Attributions of Nanoparticulate Iron Oxides, Using Symmetric Peak Component Line Shapes. *J. Phys. Chem. C* 2010, *114*, 10711−10718.

(29) Sengar, S. K.; Mehta, B. R.; Gupta, G. Charge transfer, lattice distortion, and quantum confinement effects in Pd, Cu, and Pd-Cu nanoparticles; Size and alloying induced modifications in binding energy. *Appl. Phys. Lett.* 2011, *98*, 193115.

(30) Gregg, S. J.; Sing, K. S. W. *Adsorption, surface area, and porosity*; Academic Press: London; New York, 1982.

(31) McNaught, A. D.; Wilkinson, A. International Union of Pure and Applied Chemistry. *Compendium of Chemical Terminology: IUPAC Recommendations*; Blackwell Science: Oxford [England] and Malden, MA, USA, 1997.

(32) Heuchel, M.; Jaroniec, M. Use of Simulated Adsorption Isotherms To Study Surface and Structural Heterogeneities of Microporous Solids. *Langmuir* 1995, *11*, 4532−4538.

(33) Nakazawa, M.; Somorjai, G. A. Adsorption of substituted benzenes on polycrystalline gold and on zinc oxide and iron oxide overlayers. *Appl. Surf. Sci.* 1993, *68*, 517−537.

(34) Bronstein, L. M.; Huang, X.; Retrum, J.; Schmucker, A.; Pink, M.; Stein, B. D.; Dragnea, B. Influence of Iron Oleate Complex Structure on Iron Oxide Nanoparticle Formation. *Chem. Mater.* 2007, *19*, 3624−3632.

(35) Giles, C. H.; Smith, D.; Huitson, A. A general treatment and classification of the solute adsorption isotherm. I. Theoretical. *J. Colloid Interface Sci.* 1974, *47*, 755−765.

(36) López-Cortés, C.; Osorio-Revilla, G.; Gallardo-Velázquez, T.; Arellano-Cárdenas, S. Adsorption of vapor-phase VOCs (benzene and toluene) on modified clays and its relation with surface properties. *Can. J. Chem.* 2008, *86*, 305−311.

(37) Morimoto, T.; Nagao, M.; Suda, Y. Heat of immersion of zinc oxide in organic liquids. Immersion in benzene, toluene, and chlorobenzene. *J. Phys. Chem.* 1985, *89*, 4881−4883.

(38) Glover, T. G.; Sabo, D.; Vaughan, L. A.; Rossin, J. A.; Zhang, Z. J. Adsorption of Sulfur Dioxide by CoFe2O4 Spinel Ferrite Nanoparticles and Corresponding Changes in Magnetism. *Langmuir* 2012, *28*, 5695− 5702.

(39) Hill, T.; Mozaffari-Afshar, M.; Schmidt, J.; Risse, T.; Stempel, S.; Heemeier, M.; Freund, H. J. Influence of CO adsorption on the magnetism of small Co particles deposited on Al2O3. *Chem. Phys. Lett.* 1998, *292*, 524−530.

(40) Witko, M. Oxidation of hydrocarbons on transition metal oxide catalysts quantum chemical studies. *J. Mol. Catal.* 1991, *70*, 277−333.

(41) Cwiertny, D. M.; Young, M. A.; Grassian, V. H. Chemistry and Photochemistry of Mineral Dust Aerosol*. *Annu. Rev. Phys. Chem.* 2008, *59*, 27−51.

(42) Khan, F. I.; Kr. Ghoshal, A. Removal of Volatile Organic Compounds from polluted air. *J. Loss Prev. Process Ind.* 2000, *13*, 527− 545.

(43) Blaszczak, R. J. *Choosing an adsorption system for VOC: Carbon, Zeolite, or Polymers*; Office of Air Quality Planning and Standards: Research Triangle Park, NC 27711, 1999.

(44) Gilli, G.; Scursatone, E.; Bono, R. Benzene, toluene and xylenes in air, geographical distribution in the Piedmont region

(Italy) and personal exposure. *Sci. Total Environ.* 1994, *148*, 49−56.

(45) Niu, Z.; Zhang, H.; Xu, Y.; Liao, X.; Xu, L.; Chen, J. Pollution characteristics of volatile organic compounds in the atmosphere of Haicang District in Xiamen City, Southeast China. *J. Environ. Monit.* 2012, *14*, 1145−1152.

(46) Souza, K.; Mohallem, N.; Sousa, E. Mesoporous silica-magnetite nanocomposite: facile synthesis route for application in hyperthermia. *J. Sol-Gel Sci. Technol.* 2010, *53*, 418−427.

(47) Ariya, P. A.; Khan, H. *McGill Univeristy in Montreal*, unpublished results.

(48) Flórez Menéndez, J. C.; Fernández Sánchez, M. L.; Sánchez Uría, J. E.; Fernández Martínez, E.; Sanz-Medel, A. Static headspace, solid- phase microextraction and headspace solid-phase microextraction for BTEX determination in aqueous samples by gas chromatography. *Anal. Chim. Acta* 2000, *415*, 9−20.

(49) Borm, P. J. A.; Kreyling, W. Toxicological hazards of inhaled nanoparticles–potential implications for drug delivery. *J. Nanosci. Nanotechnol.* 2004, *4*, 1−11.

(50) Dunphy Guzman K. A.; Taylor, M. R.; Banfield, J. F. Environmental Risks of Nanotechnology: National Nanotechnology Initiative Funding, 2000−2004. *Environ. Sci. Technol.* 2006, *40*, 1401−1407.